Electronic Supplementary Material (ESI) for Chemical Communications

Supporting information for:

A hydride-ligated dysprosium single-molecule magnet

Ajay Venugopal,[a] Thomas Spaniol,[a] Floriana Tuna,[b,c] Liviu Ungur,[d] Liviu F. Chibotaru,[d] Jun Okuda[a] and Richard A. Layfield[b]

[a] Institute of Inorganic Chemistry, RWTH Aachen University, Landoltweg 1, 52056 Aachen, Germany.

[b]School of Chemistry, The University of Manchester, Oxford Road, Manchester, M13 9PL, U.K.

[c]EPSRC National UK EPR Facility, Photon Science Institute, The University of Manchester, Oxford Road, Manchester, M13 9PL, UK.

[d]Division of Quantum and Physical Chemistry, Katholieke Universiteit Leuven, Celestijenlaan 200F, 3001, Belgium

---

Synthesis

General considerations

All manipulations were performed under an argon atmosphere using standard Schlenk and glove-box techniques. The solvents used for the synthesis were dried, distilled and degassed prior to use by standard methods. The starting materials $[Ln(CH_2SiMe_3)_3(THF)_3]$ (Ln = Gd and Dy) were prepared using a method similar to the synthesis of $[Y(CH_2SiMe_3)_3(THF)_3]$. Me_6tren and $[Et_3NH][B\{C_6H_3\text{-}3,5\text{-}(CF_3)_2\}_4]$ were prepared according to procedures described in reference 8 of the main article. Elemental analyses were performed by the Microanalytical Laboratory of the RWTH Aachen University.

$[Ln(Me_5trenCH_2)(\mu\text{-}H)_3Ln(Me_6tren)][B\{C_6H_3(CF_3)_2\}_4]_2$, where Ln = Gd ([1][X]$_2$) or Dy ([2][X]$_2$)

$[Et_3NH][B\{C_6H_3\text{-}3,5\text{-}(CF_3)_2\}_4]$ (0.187 mmol, 0.180 g) was added to a diethyl ether solution of $[Ln(CH_2SiMe_3)_3(THF)_3]$ (0.187 mmol, 0.118 g for Ln = Gd and 0.119 g for Ln = Dy) at −40 °C under vigorous stirring. The reaction mixture was stirred for 2 min. A diethyl ether solution of Me_6tren (0.187 mmol, 50 μL), cooled to −40°C, was added to this reaction mixture and stirred for further 3 min. The solution was degassed and treated with H_2 (1 bar) at room temperature and allowed to stand for 15 h to precipitate pale yellow crystals from this solution. Data for [**1**][X]$_2$: Yield: 0.185 g (40 %); Anal. calcd for [**1**][X]$_2\cdot Et_2O$ $C_{92}H_{96}B_2F_{48}Gd_2N_8O$: C 42.8, H 3.75, N 4.35; found: C 42.4, H 3.79, N 4.47; Data for [**2**][X]$_2$: Yield: 0.170 g (36 %); Anal. calcd for [**2**][X]$_2\cdot Et_2O$ $C_{92}H_{96}B_2F_{48}Dy_2N_8O$: C 42.6, H 3.74, N 4.33; found: C 42.1, H 3.73, N 4.24.

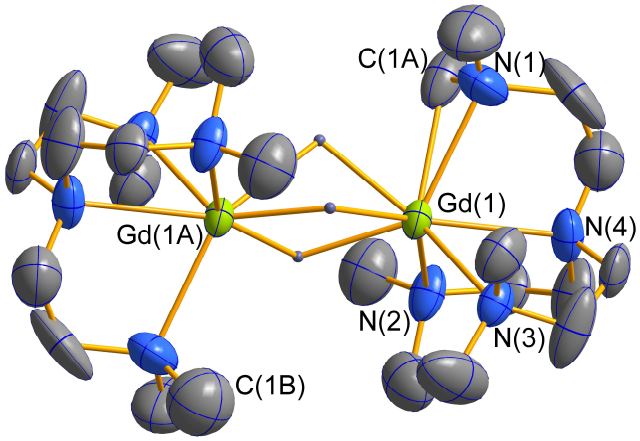

Fig. S1. Thermal ellipsoid plot (30% probability) of the structure of $[\mathbf{1}]^{2+}$. Hydrogen atoms omitted, except μ-hydride ligands.

Table S1. Crystal data and structure refinement for $[\mathbf{1}][X]_2 \cdot Et_2O$ and $[\mathbf{2}][X]_2 \cdot 2Et_2O$

	$[\mathbf{1}][X]_2 \cdot Et_2O$	$[\mathbf{2}][X]_2 \cdot 2Et_2O$
Empirical formula	$C_{92}H_{96}B_2F_{48}Gd_2N_8O$	$C_{96}H_{106}B_2Dy_2F_{48}N_8O_2$
Formula weight	2577.89	2662.51
T/K	100(2)	100(2)
λ/Å	0.71073	0.71073
Crystal system	Triclinic	Triclinic
Space group	*P*-1	*P*-1
a/Å	12.5003(11)	12.8156(8)
b/Å	14.3637(12)	13.9466(8)
c/Å	16.0369(14)	17.2860(10)
α/°	67.9589(14)	69.1184(8)
β/°	75.1829(14)	70.1955(9)
γ/°	83.3058(15)	80.8857(9)
V/Å^3	2579.6(4)	2713.4(3)
Z	1	1
Density (calculated)/Mg m^{-3}	1.659	1.629
Crystal size/mm^3	0.37 × 0.20 × 0.13	0.26 × 0.25 × 0.24
Theta range for data collection/°	2.10-29.55	2.58-30.42
Reflections collected	35157	39311
Independent reflections	13157 [*R*(int) = 0.1186]	15004 [*R*(int) = 0.0641]
Completeness/%	99.9	99.9
Data / restraints / parameters	13157 / 135 / 738	15004 / 57 / 898
Goodness-of-fit on F^2	0.942	0.868
Final *R* indices [$I>2\sigma(I)$]	*R*1 = 0.0683, *wR*2 = 0.1622	*R*1 = 0.0407, *wR*2 = 0.0675
R indices (all data)	*R*1 = 0.0989, *wR*2 = 0.1764	*R*1 = 0.0566, *wR*2 = 0.0718
Largest diff. peak and hole/e.Å^{-3}	2.473 and -1.298	1.368 and -1.271

Table S2. Selected bond lengths [Å] and angles [°] for $[\mathbf{1}]^{2+}$ and $[\mathbf{2}]^{2+}$

	$[\mathbf{1}]^{2+}$	$[\mathbf{2}]^{2+}$
Ln(1)–C(1)	2.76(3)	2.596(15)
Ln(1)–N(1)	2.514(7)	2.515(3)
Ln(1)–N(2)	2.539(6)	2.504(3)
Ln(1)–N(3)	2.581(5)	2.528(3)
Ln(1)–N(4)	2.616(6)	2.581(2)
Ln(1)–H(1)	2.11(2)	2.20(2)
Ln(1)–H(2)	2.10(2)	2.20(2)
Ln(1)–H(3)	2.11(2)	2.21(3)
Ln(1)···Ln(1A)	3.4140(6)	3.3377(3)
C(1)-Ln(1)-N(2)	32.3(4)	27.8(4)
N(1)-Ln(1)-N(2)	113.7(3)	116.01(9)
N(1)-Ln(1)-N(3)	105.5(2)	106.37(9)
N(1)-Ln(1)-N(4)	70.8(2)	70.28(9)
N(2)-Ln(1)-N(3)	106.8(2)	105.00(10)
N(2)-Ln(1)-N(4)	69.5(2)	70.42(9)
N(3)-Ln(1)-N(4)	68.92(19)	70.08(8)

Magnetic measurements

The magnetic properties of polycrystalline samples of [**1**][X]$_2$ and [**2**][X]$_2$ were measured using a Quantum Design MPMS-7 SQUID magnetometer at temperatures in the range 1.8-300 K. In a glove box, the polycrystalline samples were transferred to Kel-F capsules, which were then sealed with an O-ring cap, and the capsules were then placed in plastic straws. One end of the straw was then sealed with a cap, and the other end was sealed with Blu-Tac. The straw was then sealed in a Schlenk tube and taken to the magnetometer. The straw was removed from the Schlenk tube and the Blu-Tac quickly replaced with the carbon fibre rod, and then the sample was quickly transferred to the purged sample space of the MPMS.

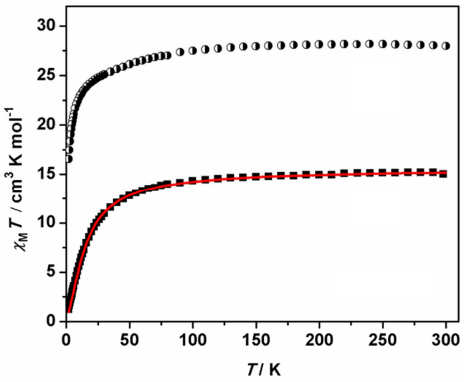

Fig. S2. Temperature dependence of $\chi_M T$ in [**1**][X]$_2$ (squares) and [**2**][X]$_2$ (circles). The solid red line is the theoretical fit of the experimental data for [**1**][X]$_2$, using the parameters described in the text.

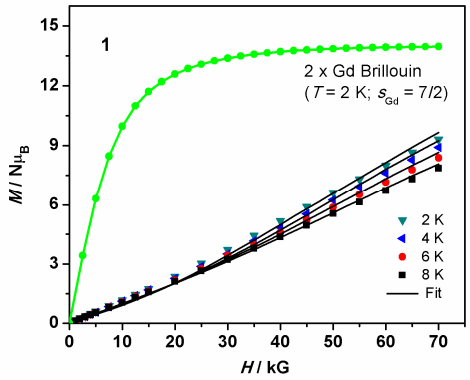

Fig. S3. Left: *M* vs. *H* for [**1**][X]$_2$ at temperatures of 2, 4, 6 and 8 K (the solid lines are theoretical fits of the experimental data using the spin Hamiltonian $H = -J[S_{Gd1} \cdot S_{Gd1A}]$ (J = –1.22 cm^{-1} and g = 1.995).

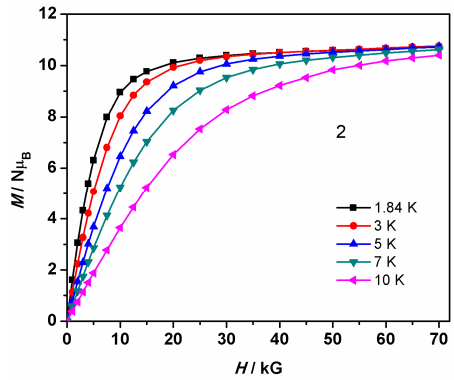

Fig. S4. *M* vs. *H* for [**2**][X]$_2$ at temperatures between 1.8 and 10 K (solid lines are a guide for the eye).

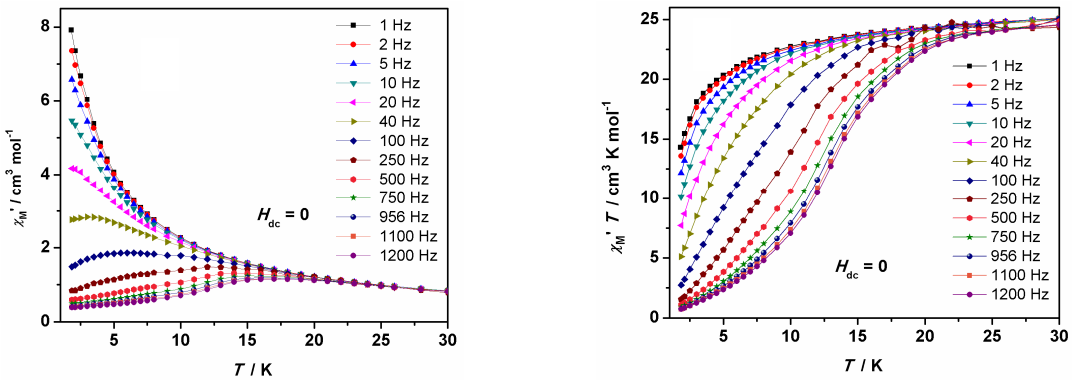

Fig. S5. Temperature dependence of the in-phase ac susceptibility of [**2**][X]$_2$ at zero-dc field and 1.55 G ac field, oscillating at the indicated frequencies.

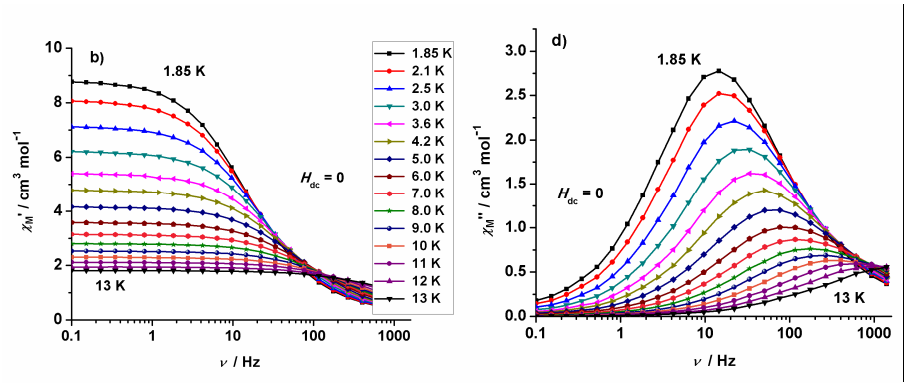

Fig. S6. Frequency dependence of the in-phase (left) and the out-of-phase (right) ac susceptibility of [**2**][X]$_2$ in zero-dc field and a 1.55 G ac field, recorded at various temperatures in the range 1.85-13 K.

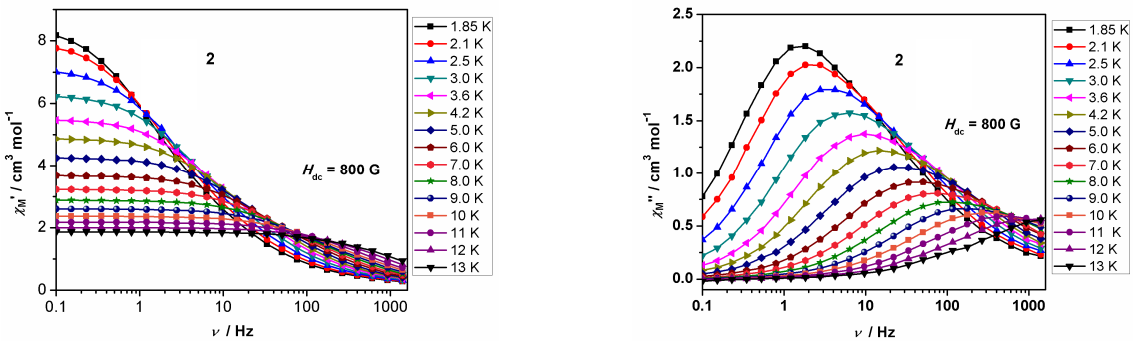

Fig. S7. Frequency dependence of the in-phase (left) and the out-of-phase (right) ac susceptibility of **2** in a dc field of 800 G and a 1.55 G ac field, recorded at various temperatures in the range 1.85-13 K.

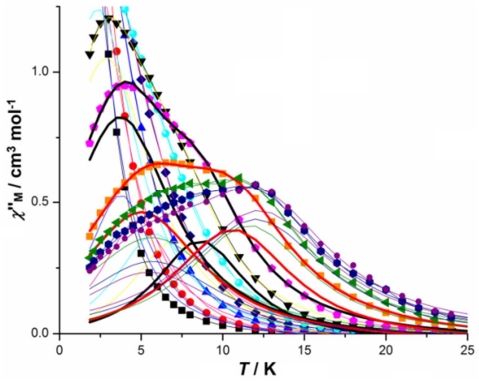

Fig S8. Deconvolution of $\chi_M''(T)$ curves for [**2**][X]$_2$ at two selected frequencies (H_{dc} = 800 G).

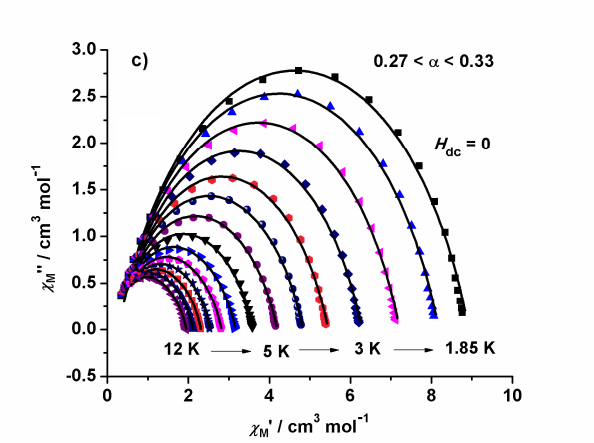

Fig. S9. Cole-Cole diagram for [**2**][X]$_2$ at temperatures in the range1.85-12 K and in zero dc field.

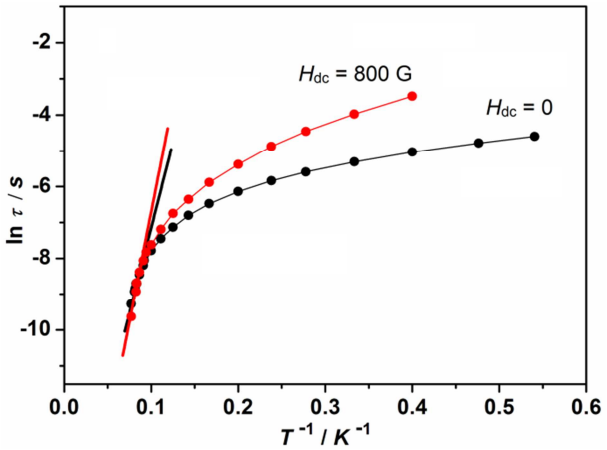

Fig. S10. Plot of ln τ *vs.* (1/*T*) for [**2**]X$_2$ in zero dc field from the $\chi_M''(\nu)$ data. The solid line is the best fit in the thermally activated regime.

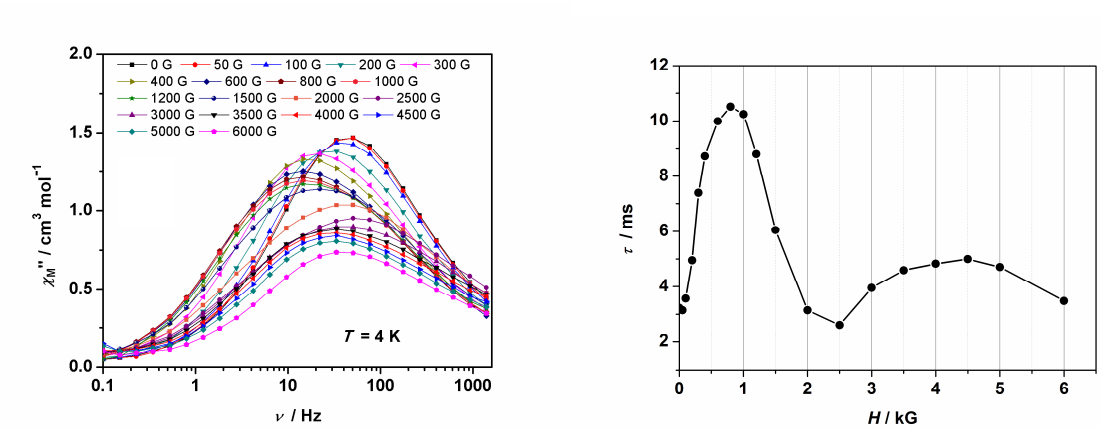

Fig. S11. Left: Frequency dependence at 4 K of the out-of-phase ac susceptibility of [**2**][X]$_2$ at several static fields. Right: Field dependence at 4 K of the relaxation time of [**2**][X]$_2$.

Ab initio study of $[2]^{2+}$

Computational details

All calculations were done with MOLCAS 7.6 and are of CASSCF/RASSI/SINGLE_ANISO type.
Two structural models for the mononuclear Dy fragments have been employed: fragment **A** (small) and **B** (large). Structure of the structural model **A** is shown in Figure 1. The model **B** has the same structure as the initial $\mathbf{[2]}^{2+}$ complex, in which the neighboring Dy ion was computationally substituted by diamagnetic Lu.

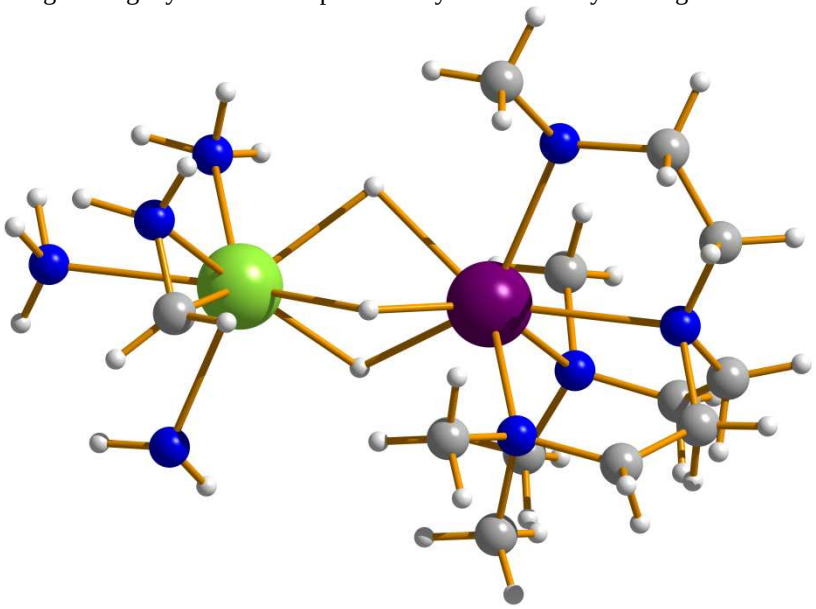

Figure S12. Structure of the fragment **A** of the Dy1. The fragment **A** of the Dy2 is similar. Color scheme: Dy – violet, Lu – green; N – blue, C – grey, H – white.

Two basis set approximations have been employed: **1** – small, and **2** – large. Table S1 shows the contractions of the employed basis sets for all elements.

Table S3. Contractions of the employed basis sets in computational approximations **1** and **2**.

Basis 1	Basis 2
Dy.ANO-RCC...7s6p4d3f1g.	Dy.ANO-RCC...8s7p5d4f2g1h.
Lu.ANO-RCC...7s6p4d3f1g.	Lu.ANO-RCC...7s6p4d3f1g.
O.ANO-RCC...3s2p1d. (close)	O.ANO-RCC...4s3p2d. (close)
O.ANO-DK3.Tsuchiya.12s8p.2s1p. (distant)	O.ANO-RCC...3s2p. (distant)
N.ANO-RCC...3s2p1d. (close)	N.ANO-RCC...4s3p2d. (close)
N.ANO-DK3.Tsuchiya.12s8p.2s1p. (distant)	N.ANO-RCC...3s2p. (distant)
C.ANO-RCC...3s2p. (close)	C.ANO-RCC...4s3p1d. (close)
C.ANO-DK3.Tsuchiya.12s8p.2s1p. (distant)	C.ANO-RCC...3s2p. (distant)
H.ANO-RCC...2s1p. (close)	H.ANO-RCC...3s2p1d. (close)
H.ANO-DK3.Tsuchiya.6s.1s. (distant)	H.ANO-RCC...2s. (distant)

Active space of the CASSCF method included 9 electrons in 7 orbitals (4*f* orbitals of Dy^{3+} ion).
We have mixed 21 sextets, 128 quartet and 130 doublet states by spin-orbit coupling.
On the basis of the resulting spin-orbital multiplets SINGLE_ANISO program computed local magnetic properties (*g*-tensors, magnetic axes, local magnetic susceptibility, etc.)

Electronic and magnetic properties of individual Dy centers

Table S4. Energies of the lowest Kramers' doublets in $[\mathbf{2}]^{2+}$ at the highest (B2) level of theory

Doublet	Dy(1)	Dy(1A)
1	0	0
2	231	94
3	395	206
4	548	307
5	706	404
6	802	460
7	958	557
8	1228	673

Table S5. Energies of the lowest Kramers doublets (cm^{-1}) of center Dy1.

A1	A2	B1	B2
0.000	0.000	0.000	0.000
118.648	108.263	102.726	94.455
225.205	234.911	207.204	205.788
329.724	338.881	311.112	306.730
426.664	428.591	408.663	403.607
482.067	484.396	463.699	460.249
550.501	605.731	537.541	556.669
675.643	708.230	660.663	673.805
3598.817	3592.687	3593.631	3586.044
3721.823	3732.758	3710.042	3710.797
3817.979	3815.470	3801.755	3795.041
3883.003	3882.688	3860.508	3849.897
3946.397	3951.044	3927.520	3921.742
4028.492	4043.483	4014.577	4016.885
4137.005	4181.544	4124.222	4137.490
6168.588	6167.648	6160.402	6153.727
6282.959	6293.707	6272.942	6271.915
6362.264	6350.973	6344.359	6329.687
6411.141	6410.455	6387.101	6376.001
6505.639	6509.374	6490.197	6485.752
6615.840	6658.107	6604.659	6616.178
8159.265	8158.009	8148.552	8139.757
8267.180	8269.420	8256.168	8252.450
8324.562	8323.063	8301.811	8284.761
8419.021	8411.661	8402.307	8392.277
8534.755	8571.841	8523.386	8532.022
9700.578	9695.790	9687.897	9676.686
9814.495	9821.727	9799.834	9790.539
9911.510	9894.053	9891.513	9873.853
10055.943	10089.207	10044.022	10050.484
…	…	…	…

Table S6. Energies (cm^{-1}) and *g* tensors of the lowest Kramers doublets (KD) of center Dy1.

KD		A1		A2		B1		B2	
		E	*g*	E	*g*	E	*g*	E	*g*
1	g_X	0.000	0.0281	0.000	0.0377	0.000	0.0476	0.000	0.0615
	g_Y		0.0528		0.0766		0.0996		0.1374
	g_Z		19.5887		19.4351		19.4140		19.2638
2	g_X	118.648	0.2967	108.263	0.2401	102.726	0.3695	94.455	0.3650
	g_Y		0.3873		0.2807		0.4494		0.4158
	g_Z		16.5392		16.5896		16.3838		16.2353
3	g_X	225.205	1.2024	234.911	1.6631	207.204	1.3091	205.788	1.5831
	g_Y		1.4311		1.8242		1.6098		1.7524
	g_Z		13.1975		13.4035		13.1693		13.3997
4	g_X	329.724	3.2615	338.881	3.4645	311.112	3.2522	306.730	2.7588
	g_Y		4.8513		5.3142		5.0948		5.0001
	g_Z		9.3973		9.1672		9.3974		9.6135
5	g_X	426.664	8.0005	428.591	0.6535	408.663	7.9117	403.607	8.4335
	g_Y		5.9070		4.1154		5.8833		5.1516
	g_Z		0.9019		11.3211		0.4804		0.0266
6	g_X	482.067	2.2699	484.396	1.6081	463.699	2.3160	460.249	2.3162
	g_Y		3.6192		3.9027		3.9950		5.2940
	g_Z		14.9327		12.8246		14.3651		12.3812
7	g_X	550.501	0.2283	605.731	0.0552	537.541	0.2192	556.669	0.1550
	g_Y		0.4767		0.0933		0.4413		0.2849
	g_Z		17.0161		17.3897		17.1009		17.1897
8	g_X	675.643	0.0023	708.230	0.0036	660.663	0.0061	673.805	0.0122
	g_Y		0.0080		0.0062		0.0134		0.0223
	g_Z		19.5786		19.7139		19.6071		19.5902

Table S7. Energies of the lowest Kramers doublets (cm^{-1}) of center Dy2.

A1	A2	B1	B2
0.000	0.000	0.000	0.000
237.405	227.222	235.076	231.396
404.256	388.349	400.443	394.498
559.473	540.728	554.171	548.428
713.485	691.235	705.934	700.459
811.121	785.240	802.218	795.874
968.357	947.918	957.887	968.211
1224.262	1204.865	1208.115	1228.115
3668.528	3659.739	3667.399	3661.639
3830.513	3815.614	3826.810	3819.440
4025.528	4004.509	4020.360	4011.859
4162.753	4136.428	4157.666	4146.703
4258.054	4232.926	4251.051	4244.321
4400.275	4377.195	4389.622	4390.395
4622.127	4598.587	4607.954	4620.043
6267.803	6252.676	6265.479	6255.464
6423.806	6405.338	6419.703	6410.397
6599.780	6575.167	6594.526	6583.236
6700.373	6673.397	6694.813	6685.116
6849.565	6824.299	6840.202	6835.438
7058.238	7032.346	7045.336	7051.502
8290.433	8270.429	8287.211	8274.453
8439.253	8417.308	8434.414	8423.610
8587.858	8559.918	8583.146	8570.199
8731.791	8705.942	8723.681	8715.474
8951.682	8924.460	8939.586	8942.379
9840.266	9817.093	9836.511	9821.907
10016.952	9991.948	10012.659	9999.197
10195.981	10168.086	10189.358	10177.318
10335.851	10308.735	10331.101	10316.769
…	…	…	…

Table S8. Energies (cm^{-1}) and *g* tensors of the lowest Kramers doublets (KD) of center Dy2.

KD		A1		A2		B1		B2	
		E	*g*	E	*g*	E	*g*	E	*g*
1	g_X	0.000	0.0167	0.000	0.0199	0.000	0.0165	0.000	0.0187
	g_Y		0.0266		0.0323		0.0260		0.0298
	g_Z		19.7401		19.7150		19.7356		19.7236
2	g_X	237.405	0.2720	227.222	0.2989	235.076	0.2637	231.396	0.2825
	g_Y		0.3857		0.4256		0.3723		0.4008
	g_Z		16.5295		16.4797		16.5318		16.5036
3	g_X	404.256	0.8537	388.349	0.9281	400.443	0.8132	394.498	0.9048
	g_Y		1.2288		1.3487		1.1876		1.3166
	g_Z		13.5809		13.5179		13.5948		13.5450
4	g_X	559.473	2.3743	540.728	2.3715	554.171	2.3742	548.428	2.3661
	g_Y		4.0435		4.1829		3.9782		4.1062
	g_Z		10.4267		10.3649		10.4661		10.3783
5	g_X	713.485	2.4106	691.235	2.4914	705.934	2.6204	700.459	2.4356
	g_Y		3.8541		4.1085		3.5482		4.1856
	g_Z		7.6468		7.5587		7.6762		7.5299
6	g_X	811.121	3.6302	785.240	10.3313	802.218	3.6392	795.874	9.7763
	g_Y		6.6738		7.1872		6.7766		7.7128
	g_Z		10.7857		3.5402		10.6416		3.4838
7	g_X	968.357	0.4358	947.918	0.3816	957.887	0.4340	968.211	0.3541
	g_Y		0.7741		0.6575		0.7681		0.5953
	g_Z		16.9240		16.9935		16.9135		17.0205
8	g_X	1224.262	0.0150	1204.865	0.0134	1208.115	0.0152	1228.115	0.0135
	g_Y		0.0256		0.0227		0.0259		0.0231
	g_Z		19.7716		19.7694		19.7644		19.7674

Table S9. Angles between the main magnetic axes of the lowest Kramers doublet obtained in different computational approximations (degrees)

center Dy1:

	A1	A2	B1	B2
A1	0.0000	31.4715	6.9919	21.3815
A2	31.4715	0.0000	24.6074	10.2136
B1	6.9919	24.6074	0.0000	14.4488
B2	21.3815	10.2136	14.4488	0.0000

center Dy2:

	A1	A2	B1	B2
A1	0.0000	0.7204	0.4441	0.8690
A2	0.7204	0.0000	0.3073	0.1592
B1	0.4441	0.3073	0.0000	0.4373
B2	0.8690	0.1592	0.4373	0.0000

Table S10. Angles between the main magnetic axes of the lowest Kramers doublets of centers Dy1 and Dy1A (degrees).

	A1	A2	B1	B2
angle	17.9076	14.8926	10.5579	4.8479

Table S11. Magnetic interactions between Dy ions in **[2]**$^{2+}$.

Ising parameters (cm^{-1}):

	model	J_{dip}*	J_{exch}	$J_{total} = J_{dip}$* + J_{exch}
molecule 1	**A1**	7.08658	-9.77364	-2.68706
	A2	4.04437	-6.50418	-2.45981
	B1	6.53139	-9.11871	-2.58732
	B2	5.15998	-7.62463	-2.46464

* -- contribution coming only from the Ising terms ~ $\hat{\tilde{s}}_{1,z}\hat{\tilde{s}}_{2,z}$ to the dipolar coupling. In the calculation of the exchange spectrum (Table S9) the dipolar interaction included all terms.

Table S12. Energies (cm^{-1}) and the corresponding tunneling gaps and g_Z values of the lowest four exchange doublet states of **[2]**$^{2+}$.

model A1		
energy	Δ_{tun}	g_Z
0.000000000	2.15730E-05	6.0661
0.000021573		
1.053669732	3.40100E-06	38.8413
1.053673133		
118.439954506	1.68794E-04	4.0727
118.440123300		
119.907320346	9.26050E-05	36.1743
119.907412951		

model A2		
energy	Δ_{tun}	g_Z
0.000000000	2.39340E-05	5.1216
0.000023934		
1.005974379	5.24600E-05	38.8208
1.006026839		
108.604977604	2.50972E-04	4.7142
108.605228576		
108.930771597	4.41593E-04	36.0020
108.931213190		

model B1		
energy	Δ_{tun}	g_Z
0.000000000	1.84950E-05	3.5488
0.000018495		
0.984404011	2.09350E-05	38.9771
0.984424946		
102.539147008	1.44491E-04	4.3859
102.539291499		
103.899045403	1.53214E-04	35.9930
103.899198617		

model B2		
energy	Δ_{tun}	g_Z
0.000000000	2.88170E-05	1.7776
0.000028817		
0.943242397	7.26710E-05	38.9495
0.943315068		
94.576685243	2.68850E-05	4.8654
94.576712128		
95.281798894	2.98817E-04	35.7375
95.282097711		

Simulation of the static magnetic properties of [2]$^{2+}$

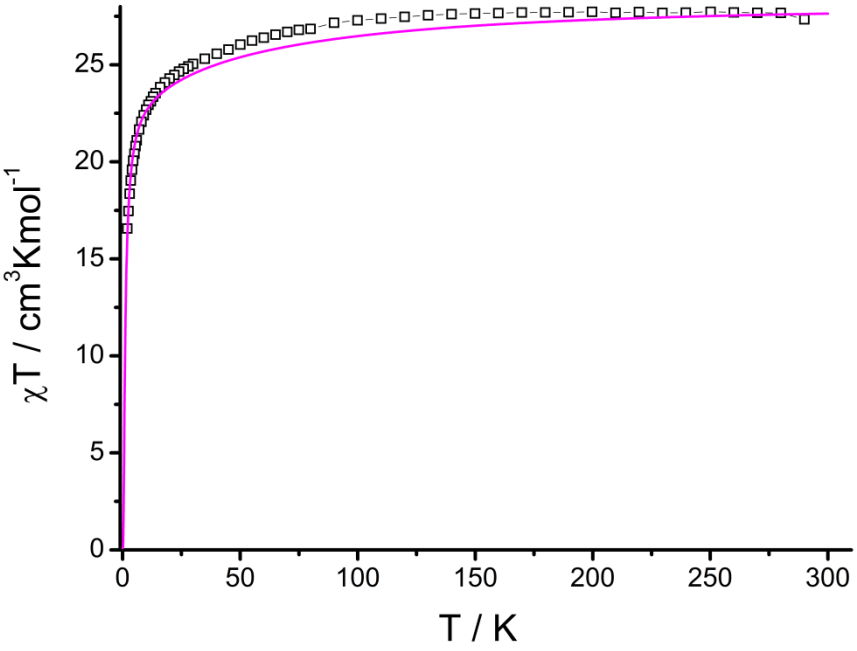

Fig. S13. Simulation of the $\chi_M T(T)$ plot for [**2**][X]$_2$ in an applied field of 1000 G.

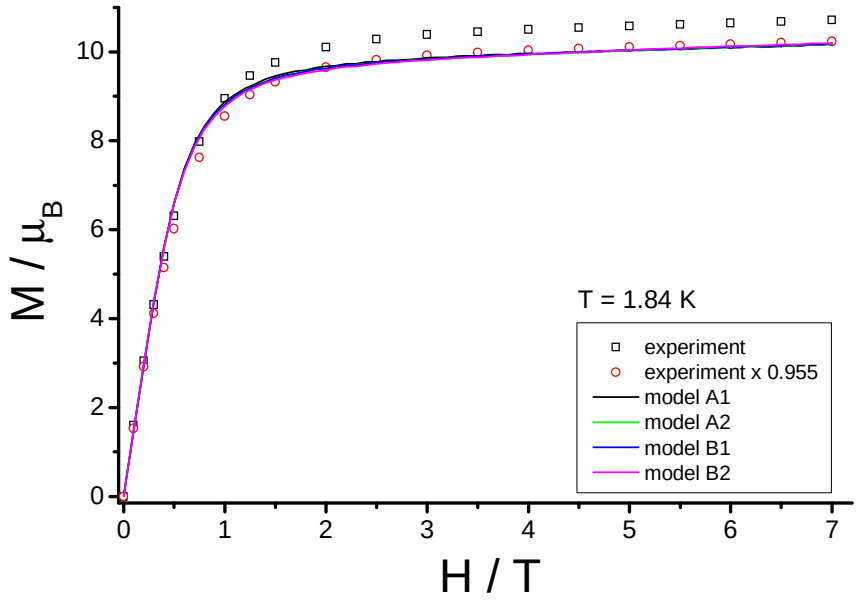

Fig. S14. Measured and calculated molar magnetization of **[2]**$^{2+}$ at 1.84 K. The downscaling of the experiment was done only to estimate the difference.

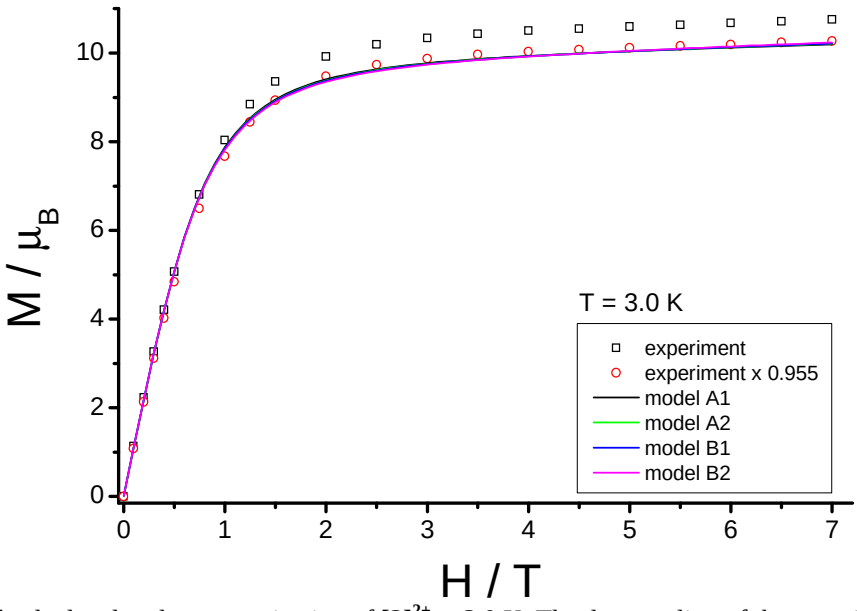

Fig. S15. Measured and calculated molar magnetization of **[2]**$^{2+}$ at 3.0 K. The downscaling of the experiment was done only to estimatethe difference.

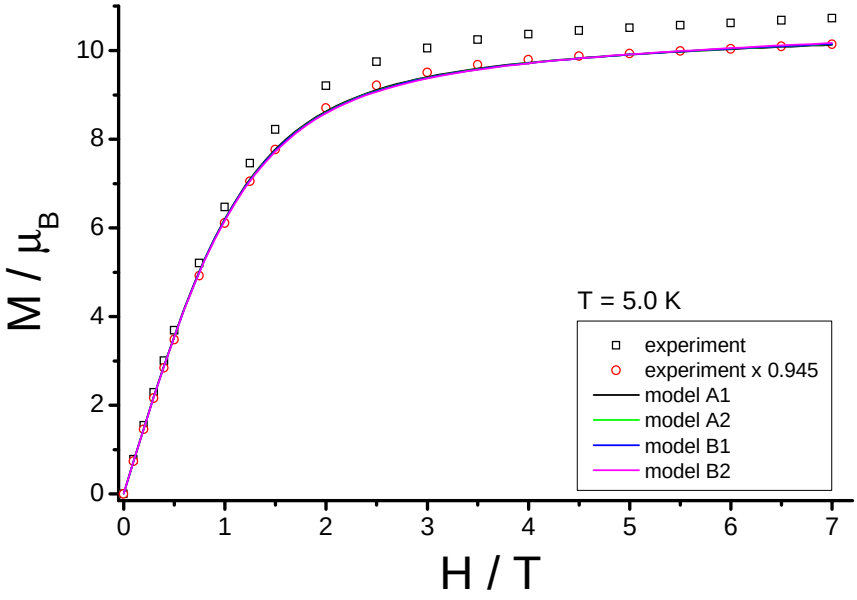

Fig. S16. Measured and calculated molar magnetization of **[2]**$^{2+}$ at 5.0 K. The downscaling of the experiment was done only to estimate the difference.

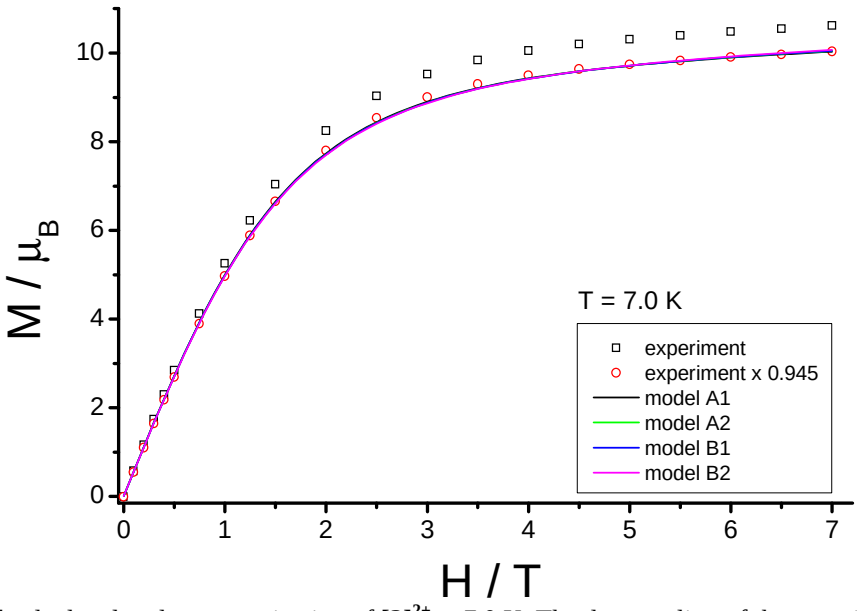

Fig. S17. Measured and calculated molar magnetization of **[2]**$^{2+}$ at 7.0 K. The downscaling of the experiment was done only to estimate the difference.

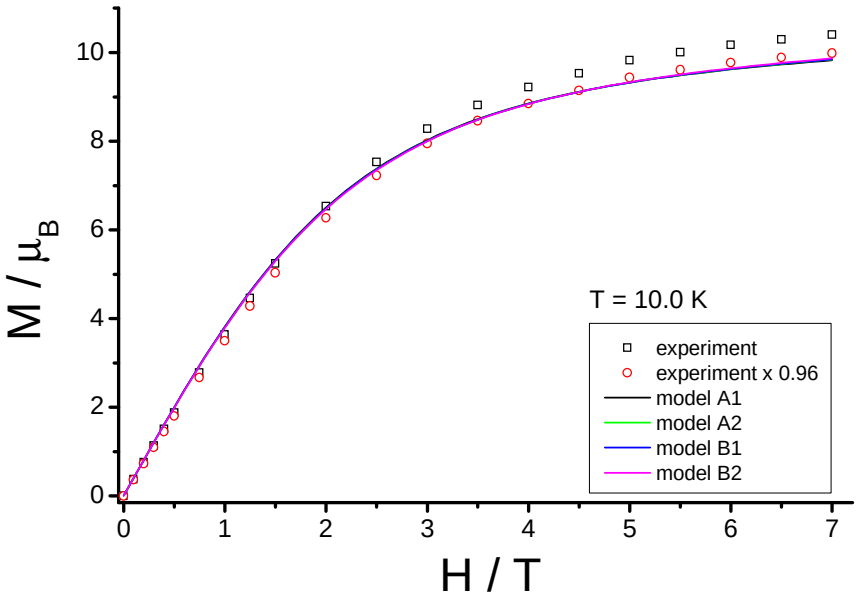

Fig. S18. Measured and calculated molar magnetization of **[2]**$^{2+}$ at 10.0 K. The downscaling of the experiment was done only to estimate the difference.